Specificity of Anion Binding in the Substrate Pocket of Bacteriorhodopsin†

Marc T. Facciotti,‡,§,|| Vincent S. Cheung,§ Christopher S. Lunde,‡ Shahab Rouhani,‡ Nitin S. Baliga,|| and Robert M. Glaeser*,‡,§

Life Sciences Division, Lawrence Berkeley National Laboratory, Berkeley, California 94720, Department of Molecular and Cell Biology, University of California, Berkeley, California 94720, and The Institute for Systems Biology, Seattle, Washington 98103

Received September 29, 2003; Revised Manuscript Received February 5, 2004

ABSTRACT: The structure of the D85S mutant of bacteriorhodopsin with a nitrate anion bound in the Schiff base binding site and the structure of the anion-free protein have been obtained in the same crystal form. Together with the previously solved structures of this anion pump, in both the anion-free state and bromide-bound state, these new structures provide insight into how this mutant of bacteriorhodopsin is able to bind a variety of different anions in the same binding pocket. The structural analysis reveals that the main structural change that accommodates different anions is the repositioning of the polar side chain of S85. On the basis of these X-ray crystal structures, the prediction is then made that the D85S/D212N double mutant might bind similar anions and do so over a broader pH range than does the single mutant. Experimental comparison of the dissociation constants, K_d, for a variety of anions confirms this prediction and demonstrates, in addition, that the binding affinity is dramatically improved by the D212N substitution.

A single point mutation, changing D85 to either threonine or serine, converts wild-type bacteriorhodopsin (bR) from what is commonly thought of as a proton pump into an anion pump shown to bind and pump a relatively broad range of substrates including chloride, bromide, and nitrate (*1*−*3*). In addition, a form of wild-type bR known as the acid-blue state, which occurs at sufficiently low pH to protonate residue 85, has also been shown to bind and pump both chloride and bromide (*1*, *4*, *5*). Thus, the possibility exists that simply neutralizing a single amino acid can convert bR from an outward-directed proton pump to an inward-directed anion pump. An alternative possibility is that wild-type bR actually pumps hydroxyl ion inward rather than pumping protons outward and that making residue 85 constitutively neutral eliminates the ability of bR to pump hydroxyl ions (*6*).

Structures of the substrate-free and bromide-bound states of bR(D85S) have already been reported to resolutions of 2.2 and 2.0 Å, respectively (*7*, *8*). Together, they illustrate how the protein adapts conformationally upon binding the halide ion. These structures also suggest how wild-type bR could use similar mechanistic principles to pump hydroxyl ions in the same direction that bR(D85S) pumps other anions.

Further understanding of how bR(D85S) functions as an ion pump can be realized by determining the structural basis for the broad anion specificity of this mutant. This type of investigation has two primary lines of interest. The first is to contribute to our understanding of how ion pumps in general bind specific substrates and how the substrate binding affinity can be modulated during the catalytic cycle. A secondary line of interest is to further investigate the implications that the anion binding geometry has for the hydroxyl ion pump model for bR.

In this study, structures are reported for a nitrate-bound form of bR(D85S) and for an anion-free form of bR(D85S), both obtained with crystals initially grown at a high chloride ion concentration. These new structures reveal how the binding site is able to accommodate chemically different substrates, i.e., nitrate ion or water, respectively. Furthermore, the dissociation constants, K_d, for bR(D85S) are determined for a variety of other anions, and these data are analyzed within the context of the water, bromide, and nitrate-bound structures of the protein. Finally, a double mutant, D85S/D212N, was predicted to show a much smaller pH dependence of anion binding. This double mutant was therefore constructed, and its anion binding behavior has been compared to that of bR(D85S). The results show that the double mutant does indeed bind anions over a wide pH range with dissociation constants as much as 270 times lower than that of bR(D85S) for identical substrates.

MATERIALS AND METHODS

Construction of the D85S/D212N Double Mutant. The *bop* gene was amplified in two segments using Hot Start KOD DNA polymerase (Novagen, Madison, WI). The first polymerase chain reaction (PCR) amplified the *bop* gene 5′-coding sequence using total DNA from the *bop* D85S mutant with the primers bop_D212_N_a (5′-CTA G*GA ATT CC*T GAC GGT TCA TCG GTT CTA A-3′) and bop_D212N_b (5′-*AAG CAC CAT GAA CAG CAG CG*T-3′). In the second PCR reaction, the 3′-end of the *bop* gene coding sequence was amplified from a wild-type copy of the *bop* gene on plasmid pNB100E (*9*) with bop_D212_N_c (5′-*CGC TGC TGT TCA TGG TGC TT***A** ACG TGA GCG CGA AGG TCG G-3′) and bop_D212N_d (5′-CTA G*GG ATC C*AT TCT ACA AGA CCG AGT GGG-3′) introducing the G→A (bold type in primer bop_D212_N_c) transition at position 473 in

† Funding for this research was provided by National Institute of Health Grant GM51487.

* To whom correspondence should be addressed. E-mail: rmglaeser@lbl.gov.

‡ Lawrence Berkeley National Laboratory.

§ University of California.

|| The Institute for Systems Biology.

10.1021/bi035757s CCC: $27.50
Published on Web 04/09/2004

the coding sequence. This changes codon 212 from GAC for aspartic acid (D) to AAC for aspargine (N). The two PCR products were subsequently fused in a third reaction by crossover PCR through the overlap (italic sequence in the bop_D212_N_b and bop_D212_N_c primers) between the two segments using primers bop_D212_N_a and bop_D212N_d to get the intact full length *bop* gene including 91 bp upstream to the start codon (*10*), the D85S and D212N mutations, and 82 bp downstream to the stop codon. The full length PCR product was cloned as an *EcoRI-BamHI* fragment (italicized nucleotides within primers bop_D212_N_a and bop_D212_N_d, respectively) by replacing a 1.2 kbp stuffer fragment in the *Escherichia coli-Halobacterium* shuttle vector pNB148 (*11*) to get plasmid pNBbopDSDN. The gene was sequenced in its entirety on both strands using primers bop_D212_N_a and bop_D212_N_d to rule out any spurious mutations introduced during PCR.

The plasmid pNBbopDSDN was transformed into *Halobacterium* sp. strain *SD23*, which has a disrupted copy of the *bop* gene (*bop*::IS*H1*) (*10*). *SD23* is an *S9* derivative and hence has a purple membrane overproducing background.

Culture Growth and Protein Isolation. Halobacterial cells expressing bR(D85S) were as used previously by Rouhani and co-workers (*7*). Expression-scale cultures of both mutants were grown as in Facciotti et al. (*12*) in the presence of 1 μg/mL Novobiocin and 20 μg/mL lovastatin (A. G. Scientific, San Diego, CA) for bR(D85S) and bR(D85S/D212N), respectively. In both cases, membranes were purified as in Facciotti and co-workers (*12*) except for the sucrose density separation step, which was in this case conducted on a continuous 32−50% gradient and fractionated into 1.5 mL fractions.

Crystallization of the D85S Mutant Protein. Purified protein was solubilized, concentrated, and crystallized as in Facciotti and co-workers (*8*). Crystals were released from the continuous bilayer gel formed by mono-olein by lipase treatment of aliquots of gel (*8*, *13*). All of the liberated crystals, initially grown in the presence 0.2M KCl, 100 mM sodium acetate, pH 4.6, and 10% PEG 4000, were transferred to a solution containing only 100 mM sodium acetate, pH 4.6, and 10% PEG 4000. This caused the crystals to visibly turn from purple to blue when viewed via a stereomicroscope, indicating that the chloride ion had left the binding site. Approximately half of the blue crystals were then soaked sequentially in cryoprotectant solutions consisting of 100 mM sodium acetate, pH 4.6, and 12, 16, 20, and 25% PEG 4000, respectively, while the second half was soaked in the same base buffers to which 1.25 M KNO_3 had been added. The crystals that were soaked in the nitrate-containing solutions turned visibly purple, thus verifying that the nitrate anion had bound.

Crystallographic Data Collection and Refinement. All crystals were then flash frozen in liquid nitrogen, and diffraction data were collected at ALS beamline 8.3.1 using a 30 μm pinhole collimator. Three crystals were used to collect the anion-free data set while two crystals were used for the nitrate-containing form. Data reduction was performed by the Elves scripts (*14*). Diffraction data were integrated with MOSFLM (*15*) and subsequently scaled with SCALA (*16*). Molecular replacement using 1KGB as the starting search model, without the retinal, water, and lipid molecules, was performed by the program CNS Version 1.1 (*17*).

Table 1: Data Collection and Crystallographic Refinement

model accession number	anion-free (1S8L)	nitrate-bound (1S8J)
data reduction resolution range (Å)	47−2.3	60−2.3
unit cell dimensions (*a*, *b*, *c*)	52.73, 121.34, 74.20	52.95, 121.08, 74.20
space group	$C222_1$	$C222_1$
total observations	111 430	160 242
unique structure factors	10 515	11 603
average $I/\sigma(I)$/high res.	9.2/6.0	7.6/3.5
completeness (%)/high res.	96.9/98.1	99.2/99.2
R_{sym}(%)/high res.[a]	10.3/19.1	14.7/23.0
refinement resolution range (Å)	12−2.3	12−2.3
number of structure factors	10 372	10 685
number of protein atoms	1714	1678
number of retinal atoms	20	20
number of water molecules	48	33
number of lipid atoms	71	49
number of nitrate atoms	N/A	4
R factor (%)[b]	21.84	21.86
R_{free} (%)[c]	25.16	23.50
average protein B (Å^2)	21.8	24.5
average retinal B (Å^2)	12.5	13.9
average water B (Å^2)	31.5	34.9
average lipid B (Å^2)	44.0	39.0
average nitrate B (Å^2)	N/A	53.6
deviation from ideal bond lengths (Å)	0.008	0.008
deviation from ideal bond angles (°)	1.0	1.0

[a] $R_{sym} = \sum_{hkl}|I_{hkl} - <I_{hkl}>|/\sum(I_{hkl})$, where *I* is the intensity. [b] *R* factor $= \sum_{hkl}|F_o - F_c|/\sum_{hkl}|F_o|$, where F_o and F_c are observed and calculated structure factors, respectively. [c] $R_{free} = \sum_{hklT}|F_o - F_c|/\sum_{hklT}|F_o|$, calculated with the T set (5−7% of the data), which has been omitted from refinement.

Refinement with CNS and model building using the program O (*18*) together with annealed simulated omit, $|F_o| - |F_c|$, and $2|F_o| - |F_c|$ maps reduced the values of *R* and R_{free} to their final values. Any refinement involving the partial occupancy of selected groups was performed by minimizing difference electron density features in omit maps. The final models were analyzed with PROCHECK (*19*) and MOLPROBITY (*20*) and exhibited good stereochemistry. Crystallographic statistics are reported in Table 1.

pH Dependence of Halide Binding. To better characterize the effects of halide binding on bR(D85S) and the D85S/D212N mutant, we carried out the same type of substrate binding measurements that had been conducted on the D85T mutant by Tittor et al. (*3*). This work not only characterized bR(D85S) and the D85S/D212N mutant for our own experiments but also allowed direct comparisons between the binding properties of the three proteins.

To determine the pH dependence of anion binding in both the bR(D85S) and the D85S/D212N mutants, 93 μL of solutions at various pH values in either 1 M potassium bromide, 1 M potassium chloride, or 1 M potassium nitrate were mixed with 7 μL of membranes resuspended in deionized water. Concentrated sulfuric acid or sodium hydroxide was used to adjust the pH of the buffers. The amount of bound anion, at a fixed anion concentration, was measured by plotting λ_{max} (the wavelength of the absorption maximum in the visible) as a function of varying pH. The results obtained in pH titration experiments at "saturating" concentrations of anions, such as those shown in Figure 5, were fitted only moderately well by an equation of the form

$$Y = Y_o + \frac{a}{1 + e^{-(x-x_o)}} \quad (1)$$

where $Y = \lambda_{max}$ at any given pH value, "x". Y_o is the minimum value of λ_{max} when no anion is bound, and x_o is the midpoint (i.e., pK_a) of the sigmoidal titration curve that is determined as a parameter during curve fitting. The parameter "a" in eq 1, also determined as a parameter during curve fitting, corresponds to the difference between the maximum and the minimum values of the function. Equation 1 would be the functional form expected if the spectroscopic titration obeyed the Henderson−Hasselbalch equation for a simple acid, HA:

$$\mathrm{pH} = \mathrm{p}K_a + \log \frac{[A^-]}{[HA]} \quad (2)$$

provided that $Y - Y_o = [A^-]$ and $a = [HA] + [A^-]$. As will be explained later, these assumptions represent a reasonable model for the spectroscopic pH titration observed in the presence of a saturating concentration of anion, since the protonation of the titratable group is imagined to lead immediately to (is linked tightly to) the binding of anion, which in turn produces the observed shift in λ_{max}.

The spectroscopic titration is described even better by an equation of the related form, however:

$$Y = Y_o + \frac{a}{1 + e^{-(x-x_o)/b}} \quad (3)$$

where the additional parameter, b, is again determined during curve fitting. This parameter b was introduced as a result of an entirely empirical trial. The best fits of the data required values of $0.2 \leq b \leq 0.5$, rather than 1.0 as for a simple acid. All curve fits were performed with SigmaPlot version 8.0 (SPSS Inc., Chicago, IL).

Anion Binding Affinity: bR(D85S). The membranes were pelleted by centrifugation at 40 000 rpm in a Beckman Ti70 rotor for 30 min and resupended to a concentration of 1.6 mg/mL in 1.2 M sodium gluconate, 50 mM sodium phosphate, pH 5.0. Seven microliters of resuspended membrane was mixed with 93 μL of buffers composed of 50 mM sodium phosphate and 1.2 M sodium gluconate, pH 5.0, containing either potassium bromide, potassium chloride, potassium nitrate, potassium nitrite, potassium iodide, or sodium azide at various concentrations. Each sample was then transferred to a 100 μL cuvette, and spectra were measured from 520 to 620 nm in a Beckman DU640 spectrophotometer (Beckman Coulter, Fullerton, CA). The pH values of all buffers were adjusted by adding microliter amounts of concentrated sulfuric acid or sodium hydroxide. pH was measured by using a Thermo-Orion 8103BN (Thermo, Beverly, MA) electrode. As advised by the Thermo technical support, the electrode fill solution was diluted 10-fold due to the high ionic strength of the buffers. This step helped to stabilize drift in the pH measurements. Fresh electrode fill solution was used before each experiment to improve accuracy.

Fractional binding was determined by initially plotting $[1/\lambda_{max}(c) - 1/\lambda_{max}(0)]$ vs concentration c, where $\lambda_{max}(c)$ is the wavelength value of the peak of the 500−600 nm absorbance maximum for a measurement at concentration c and $\lambda_{max}(0)$ is the wavelength value of the peak of the 500−600 nm absorbance maximum for a measurement in the absence of halide. Because $\lambda_{max}(c)$ values varied (usually by no more than ±1 nm) when taking multiple readings of the same sample, five readings of $\lambda_{max}(c)$ were taken for each data point and the average value was then plotted for curve fitting. These data were then fit to the following expression for single-site saturation:

$$Y = \frac{\lambda_{max}(\infty)C}{K_d + C} \quad (4)$$

where Y is the fractional binding, c is the concentration of anion, and K_d is the dissociation constant of the anion. $\lambda_{max}(\infty)$ is a parameter determined during curve fitting that corresponds to the asymptotic value of $\lambda_{max}(c)$ at saturating substrate concentrations. The resulting value of $\lambda_{max}(\infty)$, as determined from the initial fit, was then used to recalculate the fractional saturation by plotting $[1/\lambda_{max}(c) - 1/\lambda_{max}(0)]/\lambda_{max}(\infty)$. These new plots were then refit with eq 4 to determine the dissociation constants. The experimental data fit this model of binding to independent sites well enough to provide estimates of the K_d that reflect the relative strength of binding for different ions.

Anion Binding Affinity: The D85S/D212N Mutant. Measurements of substrate binding by the D85S/D212N mutant were conducted in the same way as those of bR(D85S), with the following exceptions: (i) Because of the differences in pH dependence of λ_{max} when compared to bR(D85S), the membranes of the D85S/D212N mutant were resuspended in 1.2 M sodium gluconate and 50 mM sodium phosphate, at both pH 3.5 and pH 7.5. (ii) The spectra were measured from 270 to 700 nm and were recorded using The Win Connection Suite Software (Beckman Coulter).

Fractional binding was determined by two independent methods depending on whether the data were from the low or high pH binding experiment. For the low pH binding experiments, the fractional binding and K_d values were determined by the same method employed for the bR(D85S) binding curves. The treatment differs slightly, however, because the values of $\lambda_{max}(c)$ increase sharply at low substrate concentration before reaching a plateau value and then descending again at higher substrate concentrations. This behavior suggests that two substrate binding events occur at pH 3.5, both of which have an effect on the value of λ_{max}.

The high pH binding curves, on the other hand, were determined by plotting the substrate-dependent disappearance of the 412 nm peak of the visible absorbance spectrum (Figure 1). Although this treatment represents an oversimplification of the actual linked equilibria of anion binding and protonation of the Schiff base that must be present, it nevertheless returns a good estimate of the actual K_d values. We have fit each segment of the binding curve to eq 4 to determine the respective K_d. Because the K_d values for the low concentration segments are similar to the K_d values measured at high pH, we have inferred that both correspond to binding of anions at the Schiff base site. The second binding event, characterized by a much higher K_d, only occurs at pH values below some (unmeasured) threshold. It is likely that this second, low pH binding event does not occur at pH 7.5 because it requires the protonation of an unknown amino acid that is unprotonated at higher pH values.

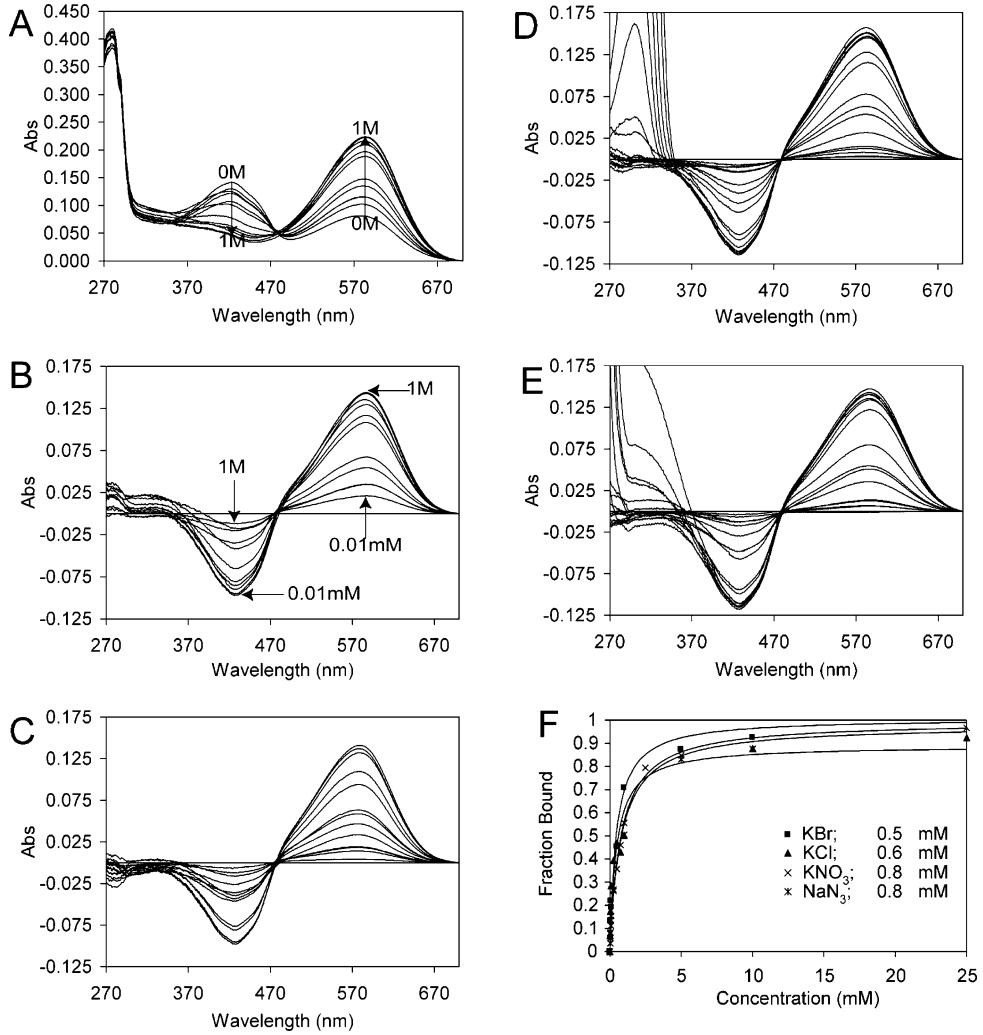

FIGURE 1: Determination of substrate binding for the D85S/D212N mutant at pH 7.5. (A) Representative spectra in the range of 270−700 nm of the D85S/D212N mutant in the presence of KBr substrate in concentrations ranging from 0 to 1 M KBr. Arrows indicate the increase and decrease of the 574 and 415 nm absorption bands, respectively, when bromide concentration is increased from 0 to 1 M. (B−E) Difference spectra calculated by subtracting the spectrum at 0 M concentration from that of each of the other spectra at the measured concentration. Panels B, C, D, and E are for bromide, chloride, nitrate, and iodide, respectively. Note that both nitrate and iodide themselves have substantial absorbance in the ultraviolet. (F) Plots of the fractional binding of the substrates shown in panels B−E. The legend notes the K_d values determined from hyperbolic curve fits of these data.

RESULTS

Structure of the Anion-Free Form of bR(D85S). The structure of bR(D85S) crystals that were grown in an anion-free form has been reported previously (*7*). Because part of the experimental procedure for soaking bromide (*8*) or nitrate ions (current work) into crystals that were grown in the presence of chloride ions involves first soaking the protein crystals in a halide-free solution to remove the chloride present during crystallization, we also had the opportunity to solve the structure of this new halide-free form of bR(D85S). This new structure allows us to observe structural changes that occur in the protein during anion binding within the same crystal form. Moreover, a comparison of this new halide-free form of bR(D85S) with the one previously solved (*7*) could also reveal what constraints the crystal packing forces impose on the conformational changes that occur as a result of anion binding and release.

The Schiff base anion binding site of bR(D85S) was previously shown to be composed of both charged and neutral polar components (*8*). Residues R82 and D212 and the protonated Schiff base contribute the charged component, while S85 and a water molecule are the main substrate-interacting, neutral species. As in the previous structure of the anion-free state, our new structure of the anion-free protein again shows a single well-ordered water molecule, water 402, bound in the anion binding pocket between the Schiff base, S85-OG, and D212-OD1 at distances of 3.11, 2.94, and 2.84 Å, respectively. The side chain of R82 is found in a downward facing conformation identical to that which is seen in the structure solved using crystals grown in the absence of halide (*7*). This conformation is stabilized by hydrogen bonds to three individual water molecules. Meanwhile, although modeling Y83 in a single conformation (similar to that of the upward facing conformation seen in the Rouhani et al. model) results in the structure with the lowest R_{free}, residual difference density suggests that the proteins in the crystal may nevertheless have a significant portion of this side chain in the more downward facing, anion-bound-like conformation. Several rounds of refinement with a dual occupancy modeled for Y83 suggest that the

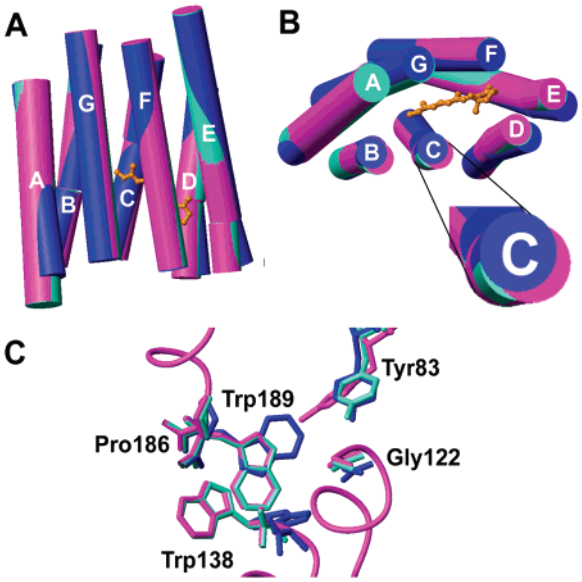

FIGURE 2: Comparison of the nitrate-bound and two water-bound structures of the D85S mutant. (A) A side view of the molecule. The extracellular side is toward the bottom. The retinal molecule is drawn in gold ball-and-stick. The magenta, green, and blue forms of the molecule represent the nitrate-bound, water-bound reported in this paper, and Rouhani et al. water-bound structure, respectively. Note that the water-bound structure reported in this paper resembles the structure of the nitrate-bound state more than that of the Rouhani et al. structure. (B) A view of the models shown in panel A from the extracellular side of the protein. Note that all of the ends of the helices for the nitrate-bound and new water-bound structure are in nearly identical positions. However, the end of helix C (enlarged) is in a position midway between the nitrate-bound and the Rouhani et al. structures. This suggests that helix C in the new water-bound structure may be trying to reach the position adopted in the Rouhani et al. structure. Note that cylinder diagrams of this sort only provide a qualitative impression of the similarities and differences between the structures; the PDB coordinate files serve as the authoritative source of information. (C) Residues 83, 122, 138, 186, and 189. The large rotamer switches seen here are a hallmark of the Rouhani et al. water-bound structure. This panel demonstrates that these key residues remain largely in the anion-bound state in the new water-bound structure rather than moving to the Rouhani et al. positions.

minor downward facing (anion-bound-like) conformation may account for roughly 30% of the occupancy. In the downward facing conformation, Y83 is hydrogen bonded to W189, while in the upward facing conformation, the side chain OH forms a hydrogen bond with the carbonyl oxygen of G119. The apparent mixture of conformations for Y83 in this structure suggests that although the conformational states of R82 and Y83 may in some way be linked, changing the conformation of Y83 is also dependent on events other than a change in conformation of R82, such as the larger repacking of helices on the extracellular side of the protein that was seen earlier by Rouhani et al. (*7*).

Backbone residue positions in this anion-free structure are very similar to those of the bromide-bound model (Figure 2A,B). The most important differences occur on the extracellular side of helix C. Starting at residue 84, the helix begins to move inward by a little more than 1 Å. The direction of movement is toward the position adopted in the crystals grown by Rouhani et al. (*7*). In addition, the end of helix C is better ordered in the halide-free crystals grown in the presence of halide than in either the bromide or the nitrate-bound forms. In fact, although the extracellular end of helix C is terminated on residue 78 in the bromide and

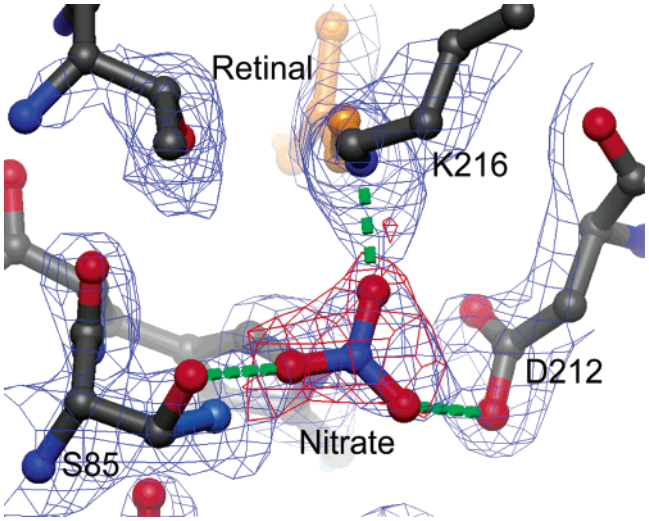

FIGURE 3: View of the nitrate substrate in the binding site of bR-(D85S). Two electron density maps are shown. In blue mesh is the $3F_o - 2F_c$ map contoured at 1.3σ while the red mesh represents the $F_o - F_c$ map contoured at 3.5σ that was calculated with the nitrate and water substrates omitted. The peak in the omit map is by far the strongest difference peak in the map. Green dashed cylinders highlight the interactions between nitrate and residues D212(OD1), S85(OG), and K216(NZ). The second minor conformer of the S85 side chain is shown in light yellow.

nitrate forms, the added ordering in the halide-free form allows interpretable electron density to residue 75. Associated with the small change in the position of helix C is the fact that residues Trp138 and Trp189, which both show large rotamer switches between the halide-free form of Rouhani et al. (*7*) and the bromide-bound form, remain in the positions of the halide-bound (ground state-like) form (Figure 2C).

Structure of the Nitrate-Bound Form. The nitrate bound form of bR(D85S) is very similar to that of the bromide-bound form in these crystals (*8*). The main structural differences are local to the anion within the binding site. The nitrate anion is bound in a position similar to that of the bromide ion and that of the water molecule in the structures discussed previously. In fact, the position of the nitrogen atom of the nitrate anion is almost superimposed on the position of the bromide. The three nitrate oxygens are closely associated with the Schiff base, S85-OG, and D212-OD1 at distances of 2.33, 2.94, and 2.84 Å, respectively (Figure 3). The short distance between the Schiff base and the nitrate oxygen suggests a close ionic interaction. It is important to note that during refinement several electron density features around the substrate, particularly in the region of the S85 side chain, suggested that the model might be best fit by modeling dual occupancy for both the substrate (nitrate and water) and the side chain of S85. Although occupancy refinement is difficult at 2.3 Å resolution, we were able to use omit maps to minimize difference density features by modeling the nitrate-bound form of the protein as 70% of the model while treating the water-bound state as 30%. We believe that the value of 70% occupancy for the nitrate anion should be regarded as being only an estimate as opposed to an accurate measurement of the occupancy.

The main adjustment made within the binding site to accommodate the larger nitrate as compared to bromide anion is a small, outward displacement of the backbone of residue 85, coupled with a rotation of the side chain around Chi1 to

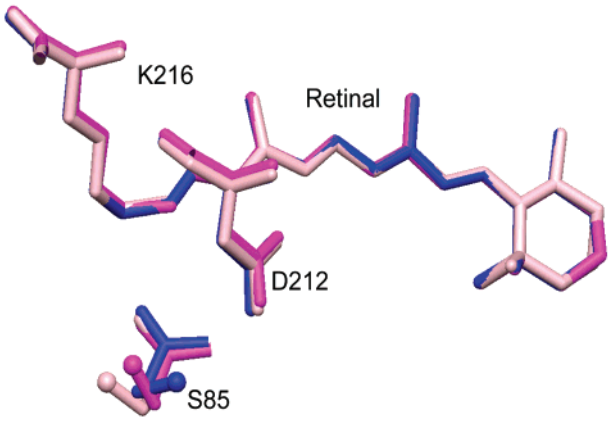

FIGURE 4: Comparison of the nitrate, bromide, and water-bound (this reference) anion binding sites of bR(D85S) shown in pink, magenta, and blue, respectively. Note that the main change in the binding site is the displacement of S85 to accommodate the differences in substrate size. To minimize confusion, the second minor conformer of the S85 side chain modeled in the nitrate-bound state is not shown as it largely overlaps the position of S85 in the anion-free state.

move OG by 1.1 Å away from where it was in the bromide-bound state (Figure 4). This movement increases the size of the binding site to accommodate the larger substrate. In addition, because unlike bromide nitrate is not spherical, the orientation of the nitrate itself must necessarily be optimized for binding. As a result, the plane made by the three oxygen atoms of the nitrate molecule is tilted somewhat relative to the plane made by the Schiff base nitrogen, S85-OG, and D212-OD1. This tilt allows the distances between the nitrate oxygens and the side chain oxygens to be physically reasonable.

Unfortunately, the electron density in the region of R82 is not easy to interpret. There is electron density visible in the region of the guanidinium group, but little to no density is visible in the region where one expects to see the CB-CG-CD linker. This situation is similar to that seen during the refinement of the bromide-bound structure. However, in the case of the bromide-bound structure, the electron density for the guanidinium group clearly suggested dual conformations that were relatively easy to model. In addition, clear density features were also visible indicating alternative positions for water molecules surrounding the side chain in the bromide-bound structure. The nitrate-bound model that produces the lowest R_{free} has the side chain of R82 100% in the downward facing conformation that is characteristic of the anion-free state. However, in this case, the $F_o - F_c$ electron density maps still reveal positive density features around the side chain that suggest missing parts of the model or multiple occupancy for the side chain. At the moment, the best conclusion that can be drawn is that the quality of the residual density in the $F_o - F_c$ map at the limited resolution of 2.3 Å is still too poor to guide us to a correct, dual occupancy model.

Anion Binding: bR(D85S). In the presence of excess anion, there is a sharp transition in the absorption spectrum as the pH is titrated between 6 and 7 (Figure 5A). The close proximity of the substrate anion to the chromophore in bR(D85S) should cause a significant change in the electrostatic environment of the conjugated π-electron system of the retinal, and we therefore presume that this is responsible

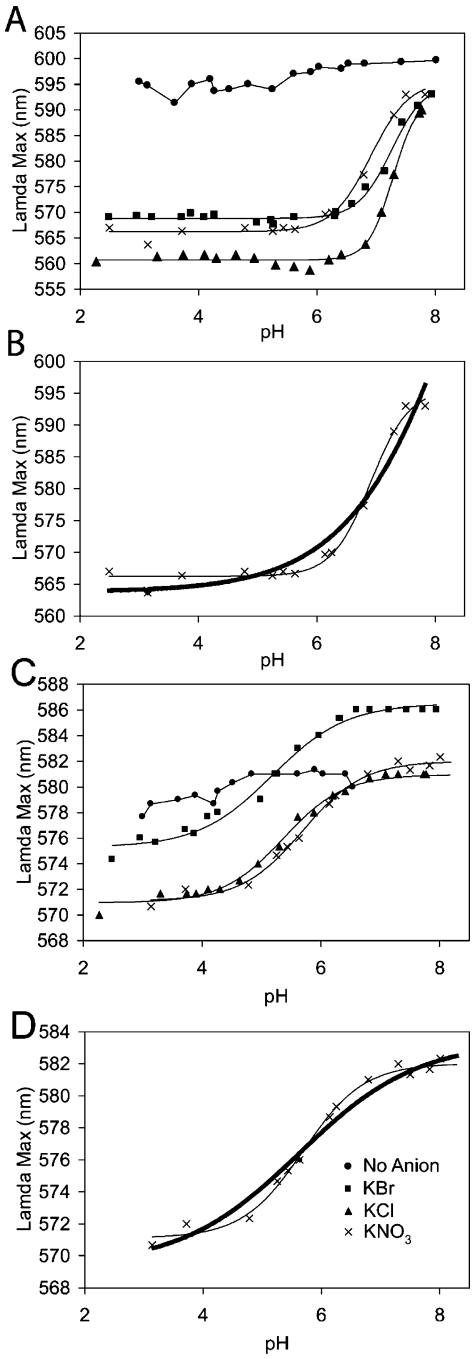

FIGURE 5: pH dependence of substrate binding in bR(D85S) and the D85S/D212N mutant. Curve fitting is described in the Materials and Methods section. (A) Curves representing the dependence of λ_{max} of bR(D85S) on pH at saturating anion substrate concentrations. (B) Curve fits of the nitrate ion data using eq 3, fixing the parameter b to one (thick line) and allowing the parameter to vary (thin line) for bR(D85S). (C) The pH dependence of λ_{max} at saturating anion substrate concentrations for the D85S/D212N mutant. (D) Curve fits of the nitrate ion data using eq 3, fixing the parameter b to one (thick line) and allowing the parameter to vary (thin line) for the D85S/D212N mutant.

for the observed blue shift in the peak of the visible light absorbance maximum of the protein. At pH values below the pK_a of the transition, the wavelength value of the 500−600 nm absorption peak (i.e., λ_{max}) is anion-dependent and stable to very low pH. At pH values slightly above the pK_a of the transition, the absorbance maxima converge asymptotically to a unique value. Above pH 8, however, the protein is destabilized and forms a yellow-colored product, which

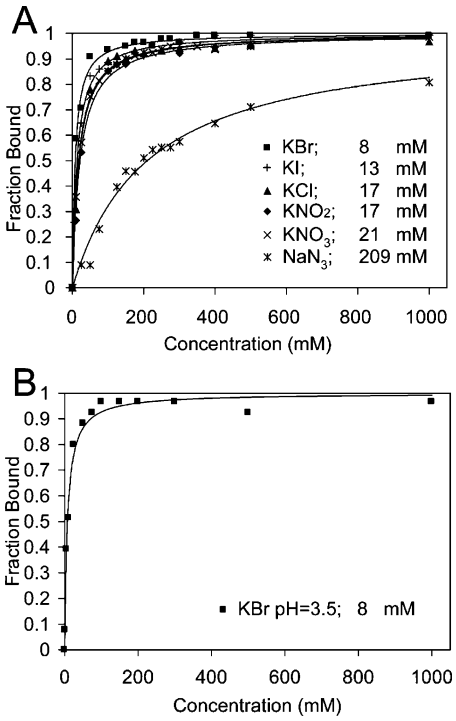

FIGURE 6: Substrate binding affinity of bR(D85S) for various anions. K_d values for the respective anions are listed in the legends. (A) Fraction of substrate bound vs anion concentration for bromide, chloride, iodide, nitrate, nitrite, and azide as measured at pH 5.0. (B) Bromide binding in bR(D85S) measured at pH 3.5. Note that the K_d value is similar to that measured at pH 5.0 showing that the binding affinity is not heavily dependent on pH at low pH values for bR(D85S).

we propose corresponds to a deprotonated Schiff base species. These data suggest that the anions shown in Figure 5 are bound at low pH but that they do not bind at pH values higher than the pK_a of the transition. Moreover, the spectral titration data are fit best when the value of the factor, *b*, which would be equal to 1 for the Henderson−Hasselbalch equation, is actually equal to 0.29, 0.21, and 0.33 for bromide, chloride, and nitrate, respectively. (Figure 5B compares the fit to the data when $b = 1$ and when *b* adopts the value that produces a best fit to the data. For clarity, only the example of nitrate is shown.) This observation suggests that titration of a key residue must be linked to the binding of an anion within the binding site. The X-ray crystal structures of both the bromide-bound and the nitrate-bound states of bR(D85S) suggest that D212 is the group that must be protonated, since neutralization of this residue would be required in order to avoid an unfavorable anion−anion interaction.

The dissociation constants for various anions at pH 5 were also determined for bR(D85S) (Figure 6A). This mutant protein binds bromide, iodide, chloride, nitrate, nitrite, and azide with decreasing specificity, the respective K_d values for these substrates being 8, 13, 17, 17, 21, and 209 mM. The most noteworthy observation is that the substrate affinities of the first five substrates differ by less than a factor of 3, whereas the K_d for azide is 10 times higher than that of the worst of the other five anions. Because the current experimental conditions are almost identical to those developed by Tittor et al. (*3*) to measure the anion affinities of the D85T mutant of bR, we can also compare our results with those of the other mutant. The dissociation constants reported for the D85T mutant of bR were 30, 80, 100, and 200 mM for azide, bromide, nitrate, and chloride, respectively. We note that with the exception of bromide, the trend in increasing K_d values for the above substrates is reversed in bR(D85S) from what it is in the D85T mutant but that the range of K_d values is similar.

Anion Binding: The D85S/D212N Mutant. On the basis of the structurally motivated hypothesis that the protonation of D212 is required for anion binding, it was anticipated that mutating residue D212 to asparagine would either reduce or eliminate the pH dependence of anion binding. Indeed, this is the case. The wavelength of the 500−600 nm absorption peak maximum, λ_{max}, is again substrate-dependent. In addition, however, λ_{max} shows a new type of pH dependence that is the same for all bound anions (Figure 5C). Furthermore, when measured at saturating halide concentration, the transition from a blue/purple color to yellow that is noted above pH 8 for bR(D85S), which is thought to be a result of Schiff base deprotonation, is not seen in the double mutant until pH values higher than 9.5 are reached. Additionally, in the anion-free state, the double mutant readily converts to a yellow species at pH 6.5 (resulting in termination of measurements reported above pH 6 in Figure 5C) while this transition is delayed and more gradual in bR(D85S). Thus, the anion specific value of λ_{max} and the protection against the transition to a yellow-colored species suggest that the anion is bound by the double mutant at all measured pH values. The double mutant exhibits similar behavior to that seen in bR(D85S) when the pH dependence of anion binding data is fit with eq 4. That is, values of $b \sim 0.3$ result in a better fit of the data than $b = 1$, suggesting that the pH titration of λ_{max} shown in Figure 5D is more complicated than the Henderson−Hasselbalch model, presumably due to a linkage with anion binding.

Because the pH dependence suggested that anion is bound over a wide range of pH values, determinations of the dissociation constants for the double mutant were made at pH values of 3.5 and 7.5. Dissociation constants for nitrite and iodide were not measured at either pH value due to difficulties in obtaining solutions of appropriate pH for these substances. For the same reason, no K_d determinations were made for azide at pH 3.5. Measurements at pH 7.5 reveal that the apparent K_d values for bromide, chloride, nitrate, and azide were not greater than 0.5, 0.6, 0.8, and 0.8 mM, respectively (Figure 1). These values are 16, 28, 21, and 261 times smaller than the K_d values for the same substrates in bR(D85S), when measured at pH 5. Because bR(D85S) loses its substrate and converts to a yellow form at pH values above 7.5, a direct comparison is not possible at this "high" pH value.

At pH 3.5, it appears that two spectroscopically detectable binding events occur. In the first, high-affinity binding event, K_d values for bromide and nitrate are 0.1 and 0.4 mM (Figure 7B), similar to the values obtained at pH 7.5, while the K_d values for the second event are 96, 120, and 223 mM, respectively, for bromide, nitrate, and chloride (Figure 7A). To verify that bR(D85S) does not show a similar, second event at low pH, a binding experiment was carried out for bR(D85S) and bromide at pH 3.5 (Figure 6B). This resulted in a single K_d value of 8 mM, identical to that determined at pH 5.

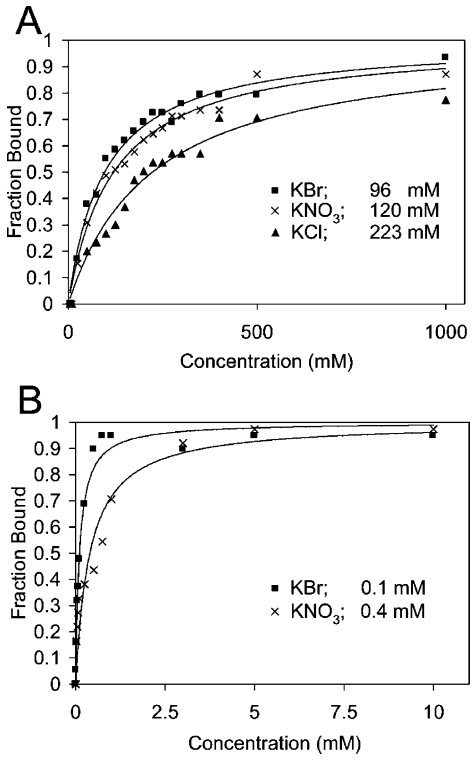

FIGURE 7: Substrate binding at pH 3.5 for the D85S/D212N mutant. (A) Data representing the blue shift in λ_{max} seen at relatively high substrate concentrations are expressed as fractional saturation vs substrate concentration. (B) Determination of fractional binding as measured by an increase in λ_{max} at low substrate concentration. The magnitude of the change in λ_{max} is relatively small (1, 6, and 6 nm for substrates chloride, bromide, and nitrate, respectively) so that reasonable determination of K_d values was only possible using this technique for bromide and nitrate. The solid lines in panels A and B represent hyperbolic curve fits to the data.

DISCUSSION

Although not entirely independent, two principle factors (the type of amino acid residues within the binding pocket and the nature of substrate-induced conformational adjustments) that affect substrate specificity and affinity have been investigated by analyzing binding affinities for various substrates in bR(D85S) and in the D85S/D212N double mutant and by comparing a new structure of bR(D85S) with nitrate bound to that of the protein with bromide bound. In addition, we can compare a similar analysis that was carried out by Tittor and co-workers (*3*) on the D85T mutant of bR. Together, these experiments reveal that small structural perturbations of the amino acids in the anion binding site of these proteins can have a considerable effect on the binding affinities toward various anionic substrates and that small structural movements within the binding site can be responsible for accommodating a relatively broad substrate specificity.

A convenient way to analyze the differences in K_d values is to compare pairs of mutants in the order of generally decreasing K_d values. We start by comparing the D85T mutant to bR(D85S). In this case, the transition from a T to S at position 85 involves only the removal of a methyl functional group. This is a relatively minor perturbation to the binding site. Indeed, it is often considered a functionally conservative substitution. However, the removal of the methyl group at position 85 results in 5−10 times lower K_d values for the same substrates. We note that if one were to order the substrates in order of decreasing K_d for both of these mutants that the trend is the same for all of the substrates except for azide. Indeed, azide has the lowest K_d of the substrates tested in the D85T mutant (30 mM) while it has the highest K_d (209 mM) for the substrates tested with bR(D85S). This dramatic change, not only in K_d but in relative binding affinity when compared to the other tested substrates, indicates just how sensitive the binding site of this anion pump is to structural perturbations. Indeed, the methyl group must therefore generally interfere with substrate binding for spherical substrates. One possibility is that T85 must orient in such a way that the methyl group sterically blocks a portion of the most favored space for substrate binding. This may result as a consequence of the reduced conformational space that the side chain of T85 can explore in the crowded binding site. However, a reduction of the volume of the binding site may actually help to bind a narrow linear substrate like azide. The exact nature of the substrate−protein interactions in the D85T mutant is, however, unknown.

The next logical comparison to make is between bR(D85S) and the D85S/D212N mutant. In this case, the structural perturbation is again relatively small. Nevertheless, anion binding in the new mutant, D85S/D212N, is much improved at both low and high pH relative to that which seen in bR(D85S) for all substrates tested. Replacing the carboxyl group with an amide group constitutively neutralizes the negative charge of a group in the binding pocket at all tested pH values. Because the mutation D to N does not significantly change the available volume of the binding site, the constitutively neutral charge and the relative polarity of the ∂-nitrogen of the asparagine R-group must therefore be the major factors that contribute to the tighter binding seen in the double mutant.

One additional experimental observation that may be explained by differences in the two side chains is the shift in the midpoint of the pH titrations of the D85S/D212N mutant relative to that of bR(D85S), under saturating anion concentrations (Figure 5). A change in λ_{max} as a function of pH would not be expected without either an anion binding event or a change in protonation state of some group around the chromophore. We believe, however, that the anion remains bound to the Schiff base throughout the pH range and is therefore not responsible for this change in λ_{max}. Experimental evidence supporting this hypothesis is the observation of the substrate type-dependent nature of the value of λ_{max} for different substrates at both high and low pH values and the substrate-mediated protection from a conversion to a yellow state at high pH values. We therefore conclude that protonation/deprotonation of one or more unknown groups must occur in the vicinity of the chromophore and that the D212N substitution shifts this pK_a to lower pH values.

However, a possible alternative explanation for the pH-dependent change in λ_{max} at saturating anion concentration that requires some consideration is that two anion binding sites are populated at low pH and that only one, presumably in the active site, is populated at high pH values. This proposal is supported by the experimental observation that the D85S/D212N mutant seems to have two distinguishable binding events that occur at low pH. A second binding site

for anions on the cytoplasmic face of the protein has already been observed in the structure of bR(D85S) (*8*). The reason the D85S/D212N double mutant seems to be spectroscopically sensitive to the binding of anions at a second site, while the D85S single mutant is not, is not clear from the available structural data.

With the exception of azide, the comparison of the binding affinities of the three mutants for a variety of anions can be understood reasonably well on a structural basis. That is, in general, binding affinities for all substrates improve when the methyl group of T85 is removed in the S85 substitution and are again improved when an additional substitution D to N is made at position 212. In addition, the trend in the order of binding affinities for different substrates is relatively constant across all mutants.

What the structures of bR(D85S), with either water, bromide, or nitrate in the binding pocket, reveal is that only a small conformational adjustment is needed within the protein to allow alternative substrates to bind. This adjustment, as one might expect, is limited to the region immediately within the binding pocket. Furthermore, this adjustment, in the case of the D85S mutants, involves movement of a single side chain (S85-OG) over a range of approximately 2.3 Å (Figure 4). Because both the 85S mutants bind bromide the best and azide the worst, we can use our chemical intuition to infer the likely reasons why the other substrates tested bind either better or worse than these two substrates. We first note that the spherical bromide ion has the best size match for the bR(D85S) binding site and that the narrow/linear nature of azide makes it a poor fit for efficient hydrogen bonding to the Schiff base, residue 85, and residue 212. Chloride, which is spherical and smaller than bromide, is perhaps too small to efficiently coordinate the three protein binding groups. Its binding is thus relatively unfavorable for the same reason that the "smaller" sodium ion is not accepted by the selectivity filter of the potassium channel (*21*, *22*). Conversely, iodide may be larger than is ideal. Nitrate seems to be relatively well-sized for this binding site and—as seen in the structure—coordinates fairly well with all three H-bonding groups. Nitrite is chemically similar to nitrate but lacks the third H-bonding group available to nitrate. Thus, it cannot coordinate within the binding site as well as nitrate and subsequently has a higher K_d value. On the other hand, nitrite's departure from linearity at least allows the doubly bonded oxygen to interact with either S85 or D212 and thus increase binding affinity in comparison to the more linear azide molecule. Such explanations are chemically sensible but ultimately must be verified by quantitative physical calculations. Nevertheless, these structures alone already imply that the small displacement of a single side chain (S85) within the substrate binding site can be responsible for conferring a broad spectrum of substrate specificity for bR(D85S).

It is worthwhile to note the apparent disparity between the saturable binding of nitrate seen in the biochemical experiments with membrane fragments and the incomplete occupancy and relatively high B-factor seen in the X-ray structure. The relatively low occupancy in the crystals suggests that the K_d in 3D crystals is significantly higher than it is in native membranes. Furthermore, although the nitrate group has a rather high B-factor, the X-ray structure gives good details that make chemical sense about the mode of binding in the crystal.

The new structure of the water-bound (anion-free) state gives some further insight into the functional role of conformational changes that occur during anion binding. For instance, the anion-free structure of bR(D85S) presented in this paper suggests that the process of removing the chloride anion (which was bound during crystallization) tends to drive the protein toward the conformation observed when it is crystallized in the absence of halide ion (*7*). However, in the new crystal form, the protein appears to be restricted (by crystal packing forces), and thus, it does not make the full transition. Nevertheless, we can still infer some mechanistic implications from the fact that partial changes in structure do occur. For example, the fact that R82 is seen entirely in the downward facing conformation as it is in the Rouhani et al. structure, rather than in a multiple occupancy state, as it is found in the anion-bound forms, reinforces the idea that two alternative conformational states of R82 are associated with the presence or absence of a negative charge at or near the position where anions bind.

The conformational change in R82 is also likely to be linked to other structural changes that occur as a result of substrate binding. A logical residue to serve as this link is Y83. This suggestion derives from the fact that Y83 seems to adopt two conformations in the anion-free state presented in this paper. Although the major conformation resembles the upward facing conformation seen in the Rouhani et al. structure, the second conformation most likely resembles that of the anion-bound forms. In the case of the anion-free structure presented in this paper, the change in conformation of R82 is not efficiently communicated to Y83 because movement of Y83 requires that it break a hydrogen bond with W189. This structural rearrangement, however, is not as favored in the anion-bound crystal packing form since the reorganization of the bonding interactions of Y83 is also associated with the reorientation of G122, W138, P186, and W189. These residues were seen to undergo significant reorientations in the comparison between the bromide-bound and the Rouhani et al. anion-free forms of bR(D85S) and were suggested to be partially responsible for determining the larger scale reorientation of the helices on the extracellular side. Yet, because of crystal packing forces, the helix displacements cannot take place when anion is removed from crystals grown in the presence of anion, thus holding the positions of the key residues listed above in the anion-bound conformation.

A picture in which R82 serves as an anion-triggered sensor and Y83 as the signal transducer to effect the repacking of helices that occurs as a result of anion uptake or release in the binding site may have some mechanistic importance for the wild-type photocycle. In the work of Rouhani et al. (*7*), we described the structure of bR(D85) crystallized in the halide-free state and discussed the implications that this structure had on the proton/hydroxyl ion pumping mechanism. That discussion treated the halide-free structure of bR(D85S) as an analogue of the O intermediate in the wild-type pumping cycle, based on the electrostatic similarities between the two states. In both, the Schiff base is protonated, residue 85 is neutral, and residue 96 is protonated. The observation that the extracellular side of the protein was more open than in the wild-type ground state suggested that

opening of the extracellular side during the O intermediate phase of the wild-type photocycle would allow for transport of hydroxyl ion to the binding site. If bR is indeed an hydroxyl ion pump, the function of the structural reorganizations involving R82, Y83, and the other key residues listed above could be to control the opening and closing of the extracellular side of the protein.

We can see that relatively small changes made within the binding site can significantly modify the binding of substrate. In the case of bR(D85S/T) mutants, anion binding affinity can vary by as much as a factor of 363 times (D85T vs D85S/D212N for chloride binding). These changes are due to relatively minor changes in the binding site—neutralization of a side chain (D212N) and the removal of a methyl group (T85S). In the case of the bR(D85S) to D85S/D212N mutation, the simple protonation of residue 212 improved binding by as much as 261 times for azide and approximately 20 times for the other measured substrates. The mechanistic implication is that small changes in a binding site can change the affinity of the site for its ligand.

In wild-type bR, the active site is known to undergo cyclic protonation/deprotonation reactions. In the proton pumping hypothesis, these reactions transfer the substrate from one group to another along a proton conduction pathway. In a hydroxyl ion pumping scheme, these reactions would represent mechanistically designed modifications of intermediate binding sites, which often maintain the OH group as a neutral water molecule by the deprotonation of one residue in the protein in concert with protonation of another residue.

Understanding the structural basis for substrate specificity in ion pumps is an important piece of the intellectual puzzle of how these protein machines function to maintain the characteristic disequilibria of ions across biological membranes. The ability, for instance, of pumps to alternate their substrate binding affinity to allow uptake of substrate from one side of the membrane but release it on the other is key to their proper function. It seems that the structural basis for such affinity modulation can arise from relatively small changes (such as protonation/deprotonation) within the binding site and perhaps from even a change of the protonation state of the substrate itself.

ACKNOWLEDGMENT

We thank Dr. Elizabeth Facciotti for her critical reading of the manuscript.

REFERENCES

1. Kalaidzidis, I. V., and Kaulen, A. D. (1997) *FEBS Lett. 418*, 239−242.
2. Sasaki, J., Brown, L. S., Chon, Y. S., Kandori, H., Maeda, A., Needleman, R., and Lanyi, J. K. (1995) *Science 269*, 73−75.
3. Tittor, J., Haupts, U., Haupts, C., Oesterhelt, D., Becker, A., and Bamberg, E. (1997) *J. Mol. Biol. 271*, 405−416.
4. Oesterhelt, D., and Stoeckenius, W. (1973) *Proc. Natl. Acad. Sci. U.S.A. 70*, 2853−2857.
5. Der, A., Szaraz, S., Toth-Boconadi, R., Tokaji, Z., Keszthelyi, L., and Stoeckenius, W. (1991) *Proc. Natl. Acad. Sci. U.S.A. 88*, 4751−4755.
6. Facciotti, M. T., Rouhani, S., and Glaeser, R. M. (2004) *FEBS Lett*. In press.
7. Rouhani, S., Cartailler, J. P., Facciotti, M. T., Walian, P., Needleman, R., Lanyi, J. K., Glaeser, R. M., and Luecke, H. (2001) *J. Mol. Biol. 313*, 615−628.
8. Facciotti, M. T., Cheung, V. S., Nguyen, D., Rouhani, S., and Glaeser, R. M. (2003) *Biophys. J. 85*, 451−458.
9. Baliga, N. S., and DasSarma, S. (1999) *J. Bacteriol. 181*, 2513−2518.
10. Yang, C. F., Kim, J. M., Molinari, E., and DasSarma, S. (1996) *J. Bacteriol. 178*, 840−845.
11. Baliga, N. S., and Dassarma, S. (2000) *Mol. Microbiol. 36*, 1175−1183.
12. Facciotti, M. T., Rouhani, S., Burkard, F. T., Betancourt, F. M., Downing, K. H., Rose, R. B., McDermott, G., and Glaeser, R. M. (2001) *Biophys. J. 81*, 3442−3455.
13. Nollert, P., and Landau, E. M. (1998) *Biochem. Soc. Trans. 26*, 709−713.
14. Holton, J. M. (2002) http://ucxray.berkeley.edu/~jamesh/elves/.
15. Leslie, A. G. W. (1992) *Joint CCP4 + ESF-EAMCB Newsletter on Protein Crystallography 26*.
16. Collaborative Computation Project, No. (1994) *Acta Crystallogr. Sect. D: Biol. Crystallogr. 50*, 760−763.
17. Brunger, A. T., Adams, P. D., Clore, G. M., DeLano, W. L., Gros, P., GrosseKunstleve, R. W., Jiang, J. S., Kuszewski, J., Nilges, M., Pannu, N. S., Read, R. J., Rice, L. M., Simonson, T., and Warren, G. L. (1998) *Acta Crystallogr. Sect. D: Biol. Crystallogr. 54*, 905−921.
18. Jones, T. A., Zou, J. Y., Cowan, S. W., and Kjeldgaard. (1991) *Acta Crystallogr. A 47*, 110−119.
19. Laskowski, R. A., Macarthur, M. W., Moss, D. S., and Thornton, J. M. (1993) *J. Appl. Crystallogr. 26*, 283−291.
20. Richardson, J. S. (2002) http://kinemage.biochem.duke.edu/molprobity/.
21. Jiang, Y., Lee, A., Chen, J., Cadene, M., Chait, B. T., and MacKinnon, R. (2002) *Nature 417*, 515−522.
22. Doyle, D. A., Morais Cabral, J., Pfuetzner, R. A., Kuo, A., Gulbis, J. M., Cohen, S. L., Chait, B. T., and MacKinnon, R. (1998) *Science 280*, 69−77.

BI035757S